J Appl Electrochem (2009) 39:569–576
DOI 10.1007/s10800-008-9694-0

ORIGINAL PAPER

Effect of sodium molybdate on the corrosion behavior of cold rolled steel in peracetic acid solution

Qing Qu · Lei Li · Shuan Jiang · Wei Bai · Zhongtao Ding

Received: 16 February 2008 / Accepted: 13 October 2008 / Published online: 2 November 2008

Abstract The effect of sodium molybdate (Na_2MoO_4) on the corrosion of cold rolled steel (CRS) in peracetic acid (PAA) solution was investigated by gravimetric measurements, Tafel polarization curves, potentiodynamic polarization and electrochemical impedance spectroscopy (EIS). All the data indicate that Na_2MoO_4 acts as a very good inhibitor in PAA solution. The inhibition efficiency increases with increasing concentration of Na_2MoO_4 and immersion time. The inhibition efficiencies, calculated from gravimetric measurements, Tafel polarization curves and electrochemical impedance spectroscopy, are in reasonably good agreement and are very similar in the three cases. Furthermore, polarization data show that Na_2MoO_4 behaves as an anodic passive type inhibitor. Fourier transform infrared spectroscopy (FTIR) and atomic force microscopy (AFM) were used to characterize the corrosion surface. A probable mechanism is presented to explain the experimental results.

Keywords Sodium molybdate · Gravimetric measurements · Tafel polarization curve · Electrochemical impedance spectroscopy · Cold rolled steel · Peracetic acid

Q. Qu (✉) · S. Jiang · Z. Ding
Department of Chemistry, Yunnan University, Kunming 650091, China
e-mail: quqing58@yahoo.com.cn

L. Li
Laboratory for Conservation and Utilization of Bio-Resources, Yunnan University, Kunming 650091, China

W. Bai
Department of Chemistry, Yunnan Nationalities University, Kunming 650092, China

1 Introduction

Peracetic acid (PAA) is a strong oxidizing acid. The increasing interest in PAA lies in its wide range of biocidal activity, in particular with respect to bacteria, algae, yeasts, moulds, fungi, and viruses. PAA is used for disinfection of schools, hospitals, factories, homes [1, 2] and also as an epoxidizing agent [3]. During the last decade, following increased interest in employing PAA as an alternative disinfectant to chlorination, some studies have investigated the technical, economic, and chemical suitability of PAA for disinfecting municipal wastewater to be reused in agriculture [4–6]. However, PAA solutions are also highly corrosive to some metals.

The cost of inorganic inhibitors is low, but most are toxic e.g., chromate, mercuride, nitrite, arsenate etc. [7]. As an environmentally acceptable and effective corrosion inhibitor for zinc, galvanized steel, and other metals, molybdate ion (MoO_4^{2-}) has been widely investigated in a variety of corrosive media [8–16]. Robertson [8] first studied the mechanism of the inhibitive effect of MoO_4^{2-} on the corrosion of carbon steel in neutral solution. Pryor and Cohen [9] extended Robertson's work to study the inhibitive mechanism. Besides steel, titanium in acidic media, [10] and zinc in NaCl solutions [11] have been protected against corrosion using MoO_4^{2-}. Furthermore, the synergism between MoO_4^{2-} and other organic and inorganic compounds for corrosion reduction has also been reported [12–14]. Recently, the inhibitive behavior of MoO_4^{2-} in acid solution [15] and simulated cooling water [16] also has been investigated, the results of which indicate that MoO_4^{2-} acts as a good inhibitor. But up to now there is no agreement on the mechanism of its action. This has been ascribed to adsorption [17] followed by partial reduction [18, 19] or the formation of insoluble complexes with the corrosion

products [20, 21]. Additionally, the suggestion of MoO_4^{2-} acting as a normal passivator has also been expressed [22]. However, the most favorable opinion for its mechanism is that MoO_4^{2-} ion is non-oxidizing though it is classified as an anodic inhibitor like chromate [23, 24]. So its successful use requires the presence of either oxygen or other oxidizing agents [25–27]. To further investigate the inhibitory capability of MoO_4^{2-} in the presence of oxidizing agent, it is very significant to study the corrosion behavior of metals in PAA solution in the presence of MoO_4^{2-} due to the strong oxidizing properties of PAA. However, literature available to date on the corrosion mechanism of metals in PAA containing MoO_4^{2-} is very scant.

The objective of this investigation is to determine the effect of Na_2MoO_4 on the corrosion of cold rolled steel (CRS) in PAA solution. A probable inhibitive mechanism is presented to explain the results.

2 Experimental

2.1 Materials

The experiments were performed with cold rolled steel (CRS) specimens with the following chemical composition (wt%): C ≤0.05, Si ≤0.02, Mn ≤0.28, S ≤0.023, P ≤0.019, Fe remainder.

The aggressive solution, 0.5% PAA by weight, was prepared by dilution of 18.4% PAA by weight. Sodium molybdate (Na_2MoO_4) used were of analytical grade. All solutions were prepared from distilled water.

2.2 Gravimetric measurements

Prior to experiments, three parallel CRS sheets of 25 × 20 × 1 mm size were successively polished using emery papers from 100 to 1,000 grade. Then, the specimens were washed with distilled water and degreased with acetone and dried with a cold air blaster. After weighing accurately, the specimens were immersed in 250 mL beakers containing 0.5% PAA in the absence and presence of different concentrations of Na_2MoO_4 for 4 h. The samples were then taken out and subsequently immersed in ASTMG1-90 standard solution (Clark solution: 100 mL HCl + 2% Sb_2O_3 + 5% $SnCl_2$) to remove the corrosion products, then washed with distilled water and acetone, dried and reweighed accurately.

2.3 Electrochemical measurements

A three-electrode system including a working electrode, an auxiliary electrode and a reference electrode was used for electrochemical measurement in 250 mL solution. The working electrodes were embedded in a PVC holder using epoxy resin giving an exposed surface of 1.0 cm^2.

Each sample was successively polished using SiC emery papers from 100 to 1,000 grade, then rinsed with distilled water, degreased with acetone, and dried with a cold air blaster. The auxiliary electrode was a platinum foil and the reference electrode a saturated calomel electrode (SCE) with a Luggin capillary positioned close to the working electrode surface in order to minimize ohmic potential drop. The working electrodes were immersed in the test solutions at open circuit potential for 2 h before measurement until a steady state appeared. All the electrochemical measurements were carried out using a PAR 2263 Potentiostat/Galvanostat (Princeton Applied Research). EIS was carried out in a frequency range of 0.1–10^5 Hz using a 10 mV peak-to-peak voltage excitation. The Tafel polarization curves were produced by polarizing to ±250 mV with respect to the free corrosion potential (E_c vs. *SCE*) at a scan rate of 0.5 mV s^{-1}. And the potentiodynamic polarization curves were carried out by polarizing in the range between −250 and 1,600 mV with respect to E_c versus *SCE* at a scan rate of 2.0 mV s^{-1}. Each experiment was repeated at least three times to check the reproducibility.

2.4 AFM studies

Prior to monitoring the topographic changes of the electrode surface, the steel specimens were abraded with emery paper from 100 to 1,000 grade, and then washed with distilled water and acetone. After immersion in PAA without and with Na_2MoO_4 at 20 °C for 4 h, the specimens were cleaned with distilled water and acetone, dried with a cold air blaster, and then used for atomic force microscope examinations performed with a SPA-400 AFM (Seiko Instrument Inc.).

2.5 FTIR studies

After immersion in PAA without and with Na_2MoO_4 at 20 °C for 4 h, the specimens were taken out and dried. The surface film was scratched carefully and the product obtained was thoroughly mixed so as to make it uniform. Model Magna-IR 560 FTIR was used to measure the spectra from the KBr wafer of the corrosion product. All the spectra in these experiments were obtained by adding 64 interferograms at a resolution of 8 cm^{-1} in the region 650–4,000 cm^{-1}.

3 Experimental results and discussion

3.1 Gravimetric measurements

The average weight loss of the steel specimens in PAA in the absence and presence of Na_2MoO_4 was

determined after 4 h immersion at 20 °C. The inhibition efficiency (IE_g) was calculated by the following equation:

$$IE_g/\% = \frac{W_0 - W}{W_0} \times 100 \quad (1)$$

where W_o and W, which were obtained by means of the average weight of three parallel specimens before and after immersion, are the average weight loss of the specimen in the absence and presence of Na_2MoO_4, respectively. The average weight before immersion (G_0) and after immersion (G) in different solutions, the corresponding average weight loss and values of IE_g and corrosion rate (CR) are listed in Table 1. Figure 1 shows the inhibition efficiency (IE_g) from the gravimetric measurements as a function of Na_2MoO_4 in PAA at 20 °C. When the concentration of Na_2MoO_4 is less than or equal to 200 mg L^{-1}, the IE_g increases sharply with increase in concentration, and a further increase causes no appreciable change in performance. Here IE_g stays around 98%. This phenomenon indicates that increasing the concentration of Na_2MoO_4 results in increasing inhibition efficiency but the higher IE_g only occurs in the presence of higher concentration of Na_2MoO_4.

Assuming the increase in inhibition is caused by adsorption of inhibitor on the steel surface and obeys the Langmuir adsorption isothermal equation [15, 28]:

$$\frac{C}{\theta} = \frac{1}{K} + C \quad (2)$$

where C is the concentration of inhibitor, K is the adsorptive equilibrium constant and θ is the surface coverage. θ was calculated from the following relation [15]:

$$\theta = \frac{W_0 - W}{W_0 - W_m} \quad (3)$$

W and W_0 are respectively the average weight loss with and without the addition of the inhibitor in PAA and W_m is the smallest average weight loss. A straight line was obtained

Table 1 Corrosion parameters obtained from weight loss of CRS in PAA containing different concentrations of Na_2MoO_4 at 20 °C

$C_{Na_2MoO_4}$(mg L^{-1})	G_0 (g)	G (g)	W (g)	CR (g m^{-2} h^{-1})	IE_g (%)
0	3.5621	3.3373	0.2248	56.21	–
50	3.5591	3.4466	0.1125	28.12	48.87
100	3.5832	3.5088	0.0744	18.59	66.93
200	3.5835	3.5766	0.0069	1.73	96.93
300	3.5704	3.5666	0.0038	0.96	98.29
400	3.5793	3.5758	0.0035	0.87	98.46
500	3.5591	3.5559	0.0032	0.79	98.60

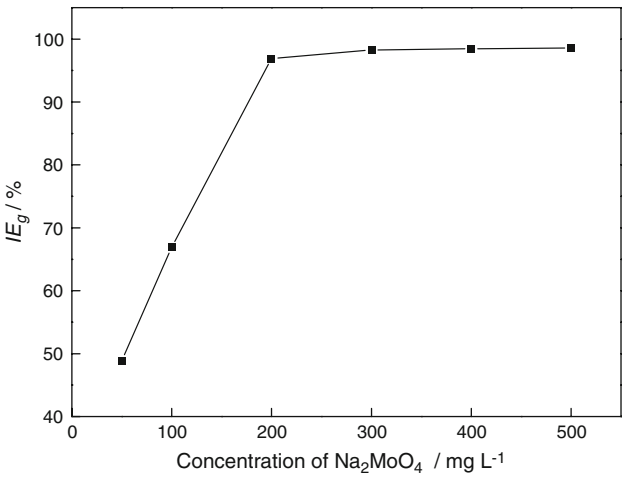

Fig. 1 Relationship between inhibition efficiency (IE_g) and concentration of Na_2MoO_4 at 20 °C

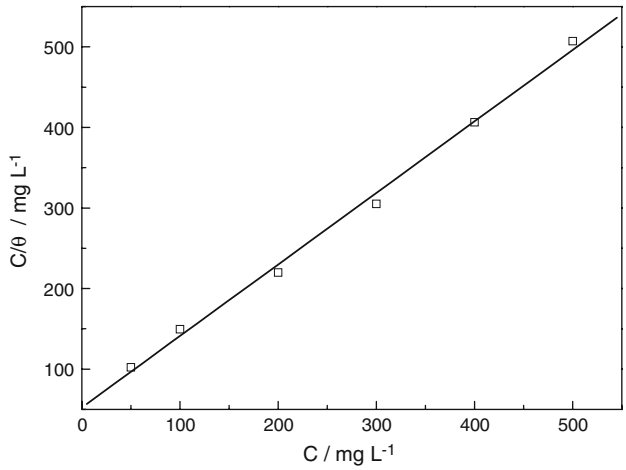

Fig. 2 Curve fitting of the corrosion data according to Langmuir thermodynamic kinetic model at 20 °C

on plotting C/θ versus C as shown in Fig. 2 suggesting that the adsorption follows Langmuir's adsorption isotherm.

Free energy of adsorption (ΔG_{ads}) was calculated using the following equation [15, 28]:

$$K = \frac{1}{55.5} \exp \frac{-\Delta G_{ads}}{RT} \quad (4)$$

The ΔG_{ads} value calculated in the presence of Na_2MoO_4 is found to be -141.95 J mol^{-1}, the negative value of ΔG_{ads} indicates that the adsorption process is spontaneous [15, 28].

3.2 Electrochemical studies

3.2.1 Polarization studies

The inhibition efficiency was obtained by the following relationship [29, 30]:

$$IE_p\% = \frac{I_{corr(o)} - I_{corr(inh)}}{I_{corr(o)}} \times 100 \quad (5)$$

where $I_{corr(o)}$ and $I_{corr(inh)}$ are the corrosion current density values in the absence and presence of inhibitor, respectively.

The potentiodynamic polarization parameters including corrosion potential (E_{corr} vs. *SCE*), corrosion current density (I_{corr}) and the inhibition efficiency (IE_p) are listed in Table 2. Figure 3 shows the Tafel polarization curves of CRS in PAA with and without Na_2MoO_4 at 20 °C. With increasing concentration of Na_2MoO_4, the corrosion potential obviously shifts positively while the curves shift to lower current densities, which results in a notably decrease in I_{corr}. This figure clearly indicates that Na_2MoO_4 acts an anodic inhibitor in PAA.

Figure 3 also indicates that active corrosion behavior is exhibited in the absence of Na_2MoO_4 while a weak passivity occurs in the presence of Na_2MoO_4. To further study the passive behavior of CRS in PAA, the potentiodynamic polarization curves in the absence and presence of 500 mg L^{-1} Na_2MoO_4 are plotted in Fig. 4. The anodic polarization current density increases rapidly with increase in potential in the absence of Na_2MoO_4. It obviously exhibits an active corrosion characteristic, while addition of 500 mg L^{-1} Na_2MoO_4 shifts the corrosion potential in the noble direction quickly, and the anodic polarization current density decreases or remains unchanged with increase in potential in the range between 0.301 and 1.319 V, which indicates that passive behavior occurs. This suggests that addition of Na_2MoO_4 in PAA gives rise to the formation of the passive film on the CRS surface and further inhibits the corrosion.

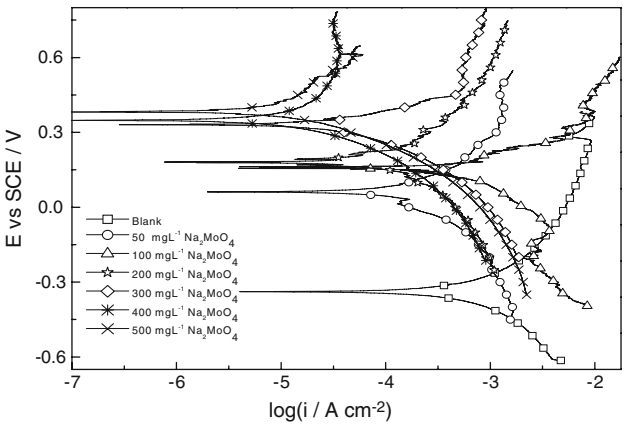

Fig. 3 Tafel polarization curves of CRS in PAA containing different concentrations of Na_2MoO_4 at 20 °C

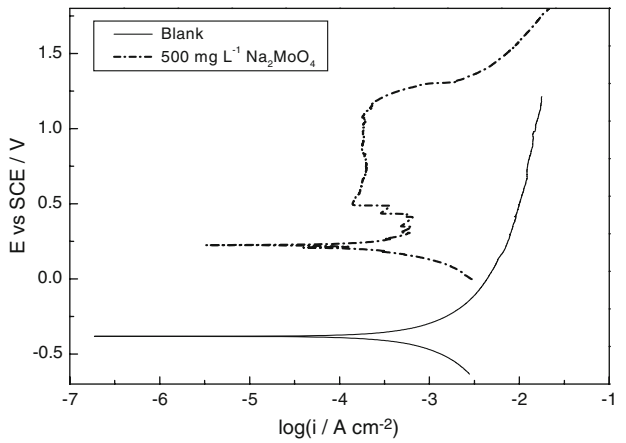

Fig. 4 Potentiodynamic polarization curves of CRS in PAA with and without 500 mg L^{-1} Na_2MoO_4

3.2.2 EIS studies

Nyquist plots of CRS in PAA with and without Na_2MoO_4 at 20 °C after 2 h immersion are given in Fig. 5. All impedance spectra exhibit one capacitive loop. However, these diagrams are not perfect semicircles which are attributed to frequency dispersion [30]. The semicircular appearance shows that the corrosion of steel is controlled by charge transfer and the presence of inhibitor does not change the mechanism of dissolution [30]. Figure 5 also indicates that the diameters of the capacitance loops in the

Table 2 Corrosion parameters obtained from electrochemical measurements of CRS in PAA containing different concentrations of Na_2MoO_4 at 20 °C

$C_{Na_2MoO_4}$ (mg L^{-1})	Polarization curves			EIS			
	E_{corr} (mV vs. SCE)	I_{corr} (μA cm^{-2})	IE_P (%)	R_s (Ω cm^2)	C_{dl} (μF cm^{-2})	R_t (Ω cm^2)	IE_{Rt} (%)
0	−338.6	550.2	–	183.2	24.0	26.0	–
50	60.4	314.1	42.92	181.1	176.4	48.5	45.83
100	154.2	200.2	63.61	172.2	56.7	150.2	82.67
200	182.3	58.7	89.33	135.2	32.0	682.9	96.19
300	330.4	19.3	96.49	147.5	28.3	766.4	96.60
400	349.0	13.3	97.58	190.2	24.5	924.1	97.19
500	385.3	11.2	97.96	193.5	23.2	937.5	97.22

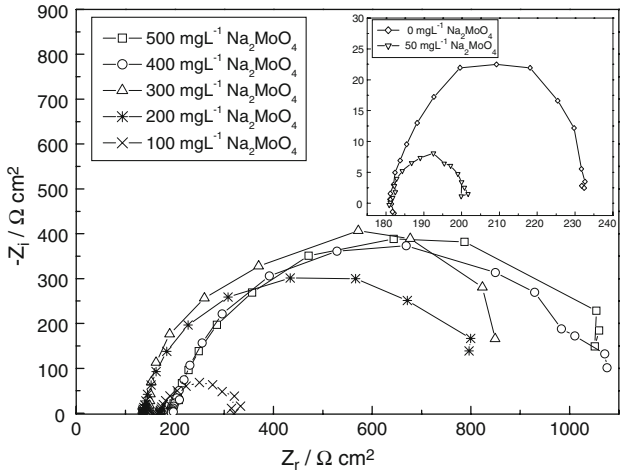

Fig. 5 Nyquist plots of CRS in PAA containing different concentrations of Na_2MoO_4 at 20 °C

presence of Na_2MoO_4 are bigger than that in the absence of Na_2MoO_4, suggesting that Na_2MoO_4 has good anti-corrosion performance in PAA.

In order to interpret the Nyquist plots more concisely, the equivalent circuit shown in Fig. 6 is proposed to simulate the results. The circuit employed allows the identification of both solution resistance (R_s) and charge transfer resistance (R_t). The double layer capacitance (C_{dl}) value is affected by imperfections of the surface which is simulated via a constant phase element (CPE) [31, 32]. A constant phase element composed of a component Q_{dl} and a coefficient α is required, and α quantifies different physical phenomena like surface non-homogeneity resulting from surface roughness, inhibitor adsorption, porous layer formation, etc. So the capacitance is deduced as follows [32]:

$$C_{dl} = Q_{dl} \times (2\pi f_{max})^{\alpha-1} \quad (6)$$

where f_{max} represents the frequency at which the imaginary value reaches a maximum on the Nyquist plot.

The inhibition efficiency was calculated by the equation:

$$IE_R/\% = \frac{R_{t(inh)} - R_{t(o)}}{R_{t(inh)}} \times 100 \quad (7)$$

where $R_{t(o)}$ and $R_{t(inh)}$ are the charge transfer resistance of CRS in PAA without and with inhibitor.

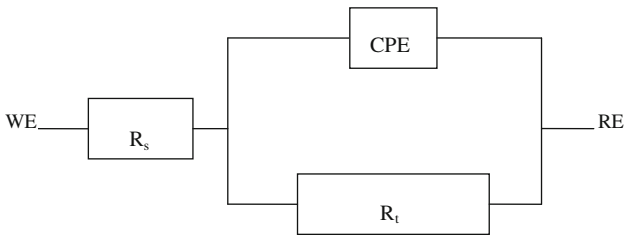

Fig. 6 Equivalent electrical circuit of EIS

The impedance parameters including C_{dl}, R_s, R_t and IE_R are listed in Table 2. With increasing concentration of Na_2MoO_4 from 0 to 500 mg L^{-1}, C_{dl} values decrease while R_t values increase. The decrease in C_{dl} and increase in R_t are related to decrease of the active surface due to inhibitor adsorption [32]. As a result, IE_R also increases markedly, which shows that Na_2MoO_4 retards the corrosion significantly. The results obtained from EIS are in good agreement with those from weight loss and Tafel polarization curves.

3.2.3 *Effect of immersion time*

Immersion time experiments were carried out in PAA with addition of 500 mg L^{-1} Na_2MoO_4 at 20 °C. Nyquist plots were recorded and are shown in Fig. 7. The diameters of the capacitance loops increase with increasing immersion time. Increase in diameter results in an increase in R_t and decrease in C_{dl}. As a result, the IE_R increases with increase in immersion time. The larger values of impedance and the character of the impedance diagrams suggest the existence of a passive film in PAA in the presence of Na_2MoO_4 [33]. The decrease in C_{dl} suggests that the film becomes thicker and more protective with increasing immersion time [32]. This further reveals that Na_2MoO_4 induces CRS passivation.

3.3 AFM studies

The AFM two-dimensional and three-dimensional images of the specimens in PAA in the absence and presence of Na_2MoO_4 are shown in Figs. 8 and 9. In the absence of Na_2MoO_4 the CRS surface looks rather uneven and appears notably potholed whereas in the presence of Na_2MoO_4 it becomes somewhat flat and close. The uneven and potholed shape indicates that the corrosion is typically electrochemical corrosion and PAA can accelerate the corrosion; while the more even surface suggests that

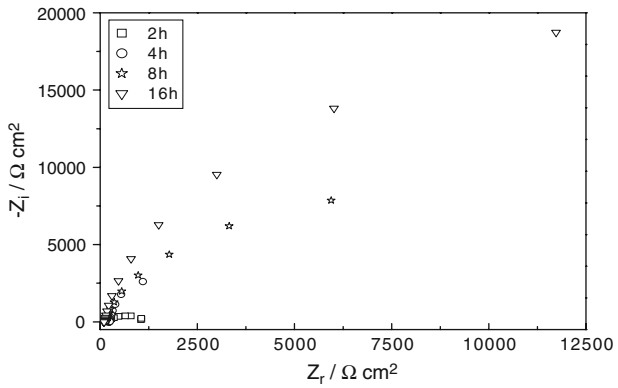

Fig. 7 Nyquist plots of CRS in PAA containing 500 mg L^{-1} Na_2MoO_4 at different immersion times at 20 °C

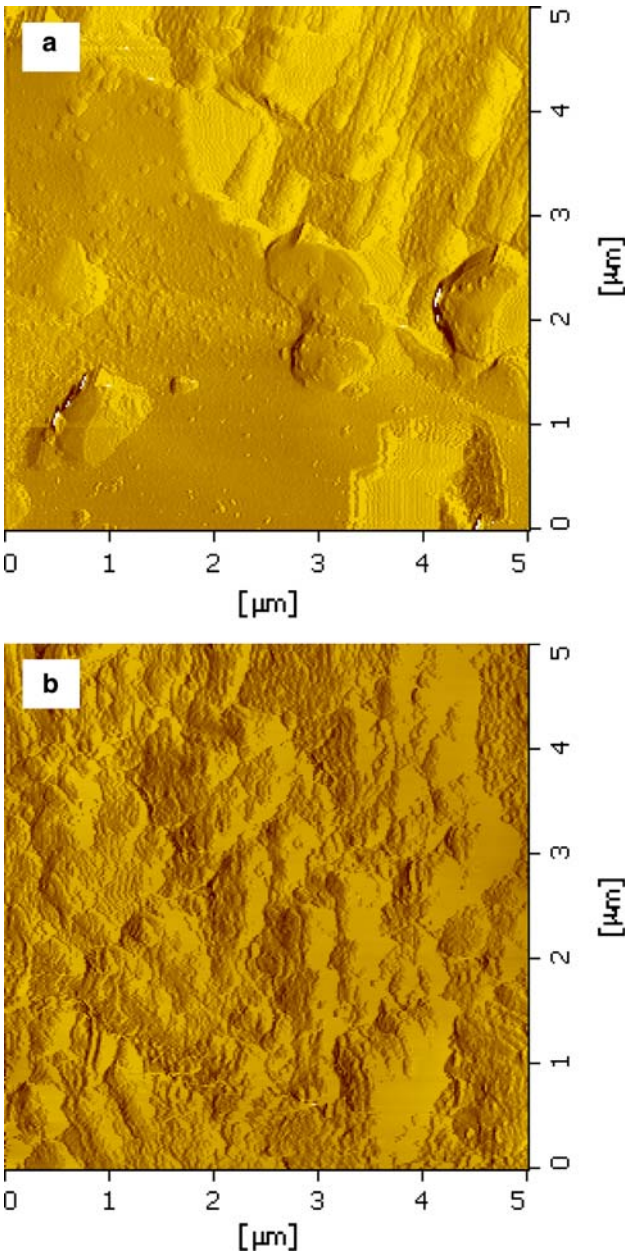

Fig. 8 AFM two-dimensional images of CRS surfaces in PAA **a** in the absence of Na_2MoO_4 and **b** in the presence of 500 mg L^{-1} Na_2MoO_4

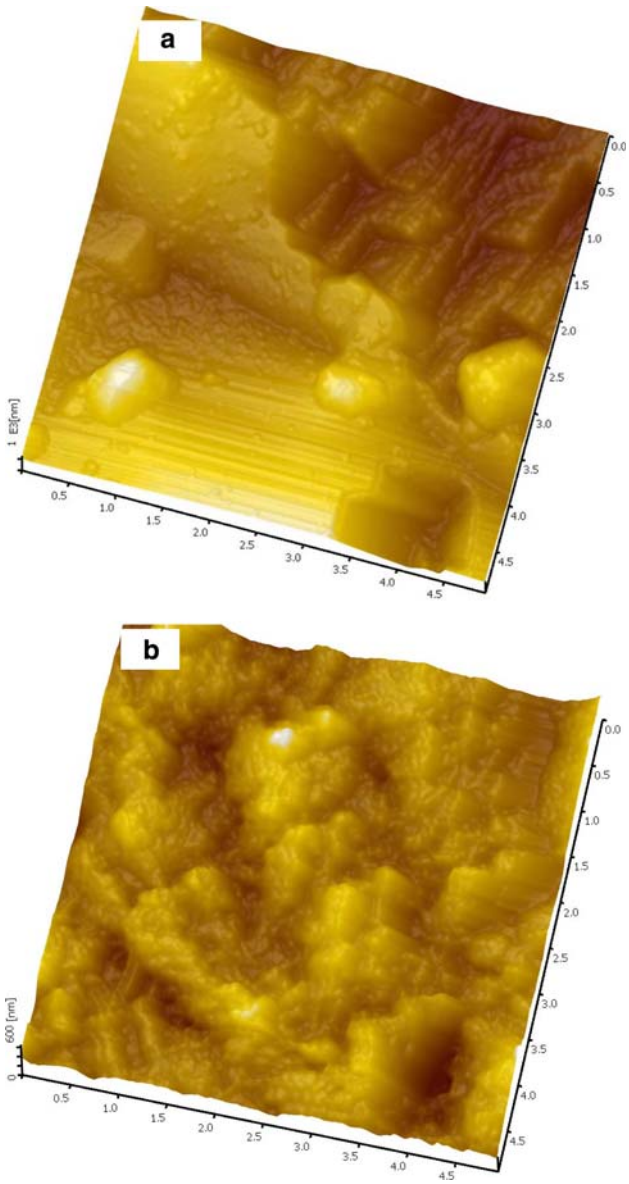

Fig. 9 AFM three-dimensional images of CRS surfaces in PAA **a** in the absence of Na_2MoO_4 and **b** in the presence of 500 mg L^{-1} Na_2MoO_4

Na_2MoO_4 in PAA can form an inhibitive film on the CRS surface.

3.4 FTIR studies

FTIR spectra of PAA and the corrosion products in the absence and presence of Na_2MoO_4 are presented in Fig. 10a, b, and c, respectively. In Fig. 10a, the broader band around 3350 cm^{-1} is attributed to O–H stretching which indicates that many PAA molecules aggregate through H-bonds, the strong band at approximately 1,710 cm^{-1} is attributed to C = O, the bands at 1,380 and 1,275 cm^{-1} can be assigned to C–H asymmetric and symmetric stretching vibrations of methyl group, the band at 720 cm^{-1} is assigned to C–H bending, and the band at 1,020 cm^{-1} is attributed to single C–O bending. In Fig. 10b, peaks at 1360 and 1,310 cm^{-1} can be attributed to C–H asymmetric and symmetric stretching vibrations of methyl group, the band at 750 cm^{-1} is assigned to C–H bending, the O–H stretching at 3,320 cm^{-1} becomes weaker which indicates that O–H is weak and no H-bonds are in the complexes, the C=O peak shifts from about 1,710 cm^{-1} to lower wavenumber (approximately 1,675 cm^{-1}) and the single C–O bending becomes rather

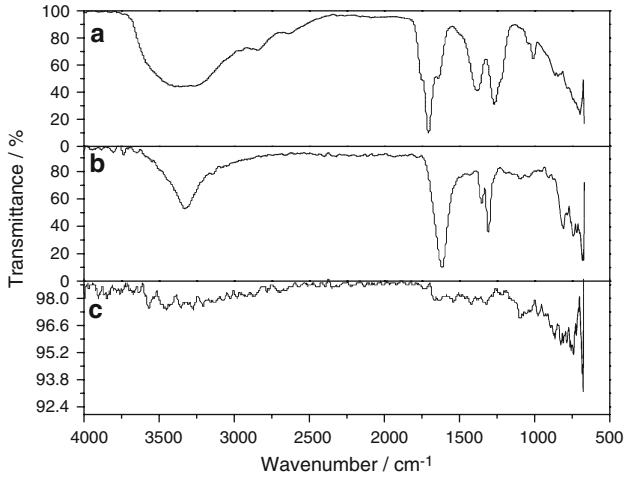

Fig. 10 FTIR spectra of **a** PAA, **b** the corrosion products of CRS in PAA in the absence of Na_2MoO_4, and **c** the corrosion products of CRS in PAA in the presence of 500 mg L^{-1} Na_2MoO_4

weak at 1,030 cm^{-1}, due to the conjugative effect of Fe–O bonds which form donor-accept surface complexes between the lone-pair electrons of oxygen and the vacant d-orbital of Fe substrate, and the peaks at 3,800 and 3,732 cm^{-1} which do not appear in Fig. 10a are assigned to Fe–O bending. FTIR analysis indicates that the adsorption of PAA ions on Fe substrate occurs in the corrosion process. The characteristic adsorption bands of Na_2MoO_4 due to Mo = O and Mo–O stretching were recorded at 897 and 831 cm^{-1} [34]. So the bands at 880 and 832 cm^{-1} in Fig. 10c may be attributed to Mo = O and Mo–O stretching in $[Fe^{2+}\cdots\cdots MoO_4^{2-}]$ or $[(HO)_4OMo–O–MoO(OH)_4]^{2-}$, the bands at 1630, 1314, 1104 and 750 cm^{-1} reveals that PAA also adsorbs onto CRS surface. However, the corresponding absorption bands of PAA become rather weak attributed to formation of the protective film $[Fe^{2+}\cdots\cdots MoO_4^{2-}]$ or competitive adsorption between $[(HO)_4OMo–O–MoO(OH)_4]^{2-}$ and CH_3COOO^-.

4 Explanation of inhibition

According to the corrosion mechanism suggested by Qu et al. [35], the dissolution of CRS in PAA in the absence of Na_2MoO_4 may be assumed as follows:

$$CH_3COOOH \rightarrow CH_3COOO^- + H^+ \quad (a)$$

$$Fe + CH_3COOO^- \rightarrow [Fe(CH_3COOO)]_{ads} + e^- \quad (b)$$

$$[Fe(CH_3COOO)]_{ads} \rightarrow [Fe(CH_3COOO)]^+ + e^- \quad (c)$$

$$[Fe(CH_3COOO)]^+ \rightarrow Fe^{2+} + CH_3COOO^- \quad (d)$$

Thus Fe^{2+} can form easily in PAA. It is well known that MoO_4^{2-} can react with Fe^{2+} to form a protective film when Na_2MoO_4 is added to PAA solution [15, 36]:

$$Fe^{2+} + MoO_4^{2-} \rightarrow \left[Fe^{2+}\cdots\cdots MoO_4^{2-}\right] \quad (e)$$

Furthermore, MoO_4^{2-} can also take the following reaction [36, 37]:

$$MoO_4^{2-} + H^+ \rightarrow MoO_3(OH)^- \quad (f)$$

$MoO_3(OH)^-$ will be coordinated with water molecules to give $MoO(OH)_5^-$, the species will further polymerize to form an oxygen-bridge:

$$2MoO(OH)_5^- \rightarrow \left[(HO)_4OMo-O-MoO(OH)_4\right]^{2-} + H_2O \quad (g)$$

$[(HO)_4OMo–O–MoO(OH)_4]^{2-}$ ions react with the blank orbit (d) of steel to form a complex, then adsorb on the steel surface to inhibit the corrosion.

5 Conclusions

The main conclusions are

(1) Na_2MoO_4 retards the corrosion of CRS in PAA. The inhibition efficiencies, calculated from gravimetric measurements, Tafel polarization curve and EIS are in reasonably good agreement.

(2) Na_2MoO_4 in PAA acts as an anodic passive type inhibitor. The inhibition is due to formation of the protective film $[Fe^{2+}\cdots\cdots MoO_4^{2-}]$ or adsorption of $[(HO)_4OMo–O–MoO(OH)_4]^{2-}$ on the steel surface.

(3) The inhibition efficiency of Na_2MoO_4 increases with increasing concentration and also with increasing immersion time.

Acknowledgements This work was financially supported by the Natural Science Foundation of China under the Grant Number 50761007, 20762014 and the Natural Science Foundation of Yunnan province under the Grant Number 2006E0008Q.

References

1. Flemmin HC (1984) Zentralbl Bakteriol Mikrobiol Hyg[B] 197:97
2. Rossoni EMM, Gaylarde CC (2000) Int J Food Microbiol 61:81
3. Wnuk SF, Lewandowsk E, Valdez CA et al (2000) Tetrahedron 56:7667
4. Kitis M (2004) Environ Int 30:47
5. Dell Erba A, Falsanisi D, Liberti L et al (2004) Desalination 168:435
6. Monarca S, Feretti D, Collivignarelli C et al (2000) Water Res 34:4261
7. Hinton BRW (1991) Met Finish 89:55
8. Robertson WD (1951) J Electrochem Soc 98:94
9. Pryor MJ, Cohen M (1953) J Electrochem Soc 100:203
10. Mitchell T (1973) US Pat 3723347
11. Hogue RD, King TM, Mitchell RS (1976) US Pat 3989637
12. Robitaille DR, Vukasovich MS (1979) US Pat 4149969

13. Lipinski RJ (1979) US Pat 4138353
14. Flynn RW, Grourke MJ (1981) US Pat 4243316
15. Mu G, Li X, Qu Q et al (2006) Corros Sci 48:445
16. Saremi M, Dehganian C, Mohammadi Sabet M (2006) Corros Sci 48:1404
17. Hunkler F, Boehni H (1983) Werks Korros 34:68
18. Bairamow AK, Zakipour S, Leygraf C (1985) Corros Sci 25:69
19. Lu A, Guo J, Zen R (1986) Huagong Jixie 13:46
20. Bairamov AK, Verdiev SC (1992) Br Corros J 27:128
21. Yalmaz VT, Sagoe-Crentsil KK, Glasser FP (1991–1992) Adv Chem Res 4:97
22. Wilcox GD, Gabe DR (1987) Br Corros J 22:254
23. Robertson WD (1951) J Electrochem Soc 98:79
24. Shams EL, Din AM, Mohammed RA, Haggag HH (1997) Desalination 114:85
25. Agarwala VS (1988) Int Corros Conf Ser NaCE-7:79
26. Sastri VS, Bednar J (1990) Mat Perform 29:44
27. Sagoe-Crentsil KK, Yilmaz VT, Glasser FP (1991–1992) Adv Cem Res 4:91
28. Bentiss F, Lebrini M, Lagrenée M (2005) Corros Sci 47:2915
29. Qu Q, Jiang S, Bai W et al (2007) Electrochim Acta 52:6811
30. Larabi L, Harek Y, Traisnel M et al (2004) J Appl Electrochem 34:833
31. Veloz MA, González I (2002) Electrochim Acta 48:135
32. Bommersbach P, Alemany-Dumont C, Millet JP et al (2006) Electrochim Acta 51:4011
33. Tanno K, Itoh M, Sekiya H et al (1993) Corros Sci 34:1453
34. Fiveash Data Management Inc (1996) FDM FTIR Spectra of Minerals and Inorganic Compounds
35. Qu Q, Jiang S, Li L et al (2008) Corros Sci 50:35
36. He ZQ (1996) J Appl Chem 13:55 (Chinese)
37. Al-Borno A, Islam M, Khraishi R (1989) Corrosion 45:970